CSIRO PUBLISHING
www.publish.csiro.au/journals/eg *Exploration Geophysics*, 2009, **40**, 1–9

Airborne electromagnetic hydrocarbon mapping in Mozambique

Andreas A. Pfaffhuber[1,4] Ståle Monstad[2] Jonathan Rudd[3]

[1]NGI, P.O. Box 3930 Ullevaal Stadion, Oslo 0806, Norway.
[2]DNO International ASA, Standen 1, Aker Brygge, Oslo 0113, Norway.
[3]Aeroquest Ltd, 7687 Bath Road, Mississauga ON, L4T 3T1, Canada.
[4]Corresponding author. Email: aap@ngi.no

Abstract. The Inhaminga hydrocarbon exploration licence in central Mozambique sets the location for a multi-method airborne geophysical survey. The size of the Inhaminga block, spanning some 16 500 km^2 from Beira to the Zambezi, limited available data and a tight exploration schedule made an airborne survey attractive for the exploration portfolio. The aim of the survey was to map hydrocarbon seepage zones based on the evidence that seepage may create resistivity, radiometric and sometimes magnetic anomalies. The survey involved a helicopter-borne time domain electromagnetic induction system (AEM) and a fixed wing magnetic gradiometer and radiometer.

Our data analysis highlights an anomaly extending some tens of kilometres through the survey area along the eastern margin of the Urema Graben. The area is imaged by AEM as a shallow resistive unit below a strong surface conductor and shows high Uranium and low Potassium concentrations (normalised to mean Thorium ratios). A seismic dimming zone on a 2D seismic line crossing the area coincides with the resistivity and radiometric anomaly. The geological exploration model expects seepage to be linked to the graben fault systems and an active seep has been sampled close to the anomaly. We thus interpret this anomaly to be associated with a gas seepage zone. Further geological ground work and seismic investigations are planned to assess this lead.

Airborne data has further improved the general understanding of the regional geology allowing spatial mapping of faults and other features from 2D seismic lines crossing the survey area.

Key words: AEM, case history, gas seepage, helicopter EM, hydrocarbons, near surface, spectrometry, TEM.

Introduction

Airborne electromagnetic (AEM) resistivity mapping has been used by the oil industry to some extent since the 1990s when airborne multi-method surveys were conducted to outline near surface alteration zones caused by hydrocarbon seepage plumes (Smith and Rowe, 1997). The correlation between hydrocarbon seepage and anomalies of the electrical properties of near surface sediments had been investigated broadly by the use of land-based EM and resistivity methods (Sternberg, 1991; Hughes, 1983). No significant activities in this field have been reported since then, however. AEM exploration for base metals has been booming over recent decades, mainly driven by a steady rise in commodity prices. Although oil and gas prices have increased significantly as well, little AEM activity has been reported in this field. Nevertheless, high energy prices enable oil and gas companies to widen their horizons and investigate the use of unconventional methods such as AEM for hydrocarbon exploration.

In early 2008 we had the opportunity to initiate a multi-method airborne geophysical survey in a petroleum exploration licence in Mozambique based on the evidence of gas seepages in the area. As a multidiscipline group consisting of Norwegian oil and gas exploration and production company DNO International ASA, geoscience research and consulting institute NGI and geophysical service and software development company PetRosEikon, we planned, and successfully conducted, the survey over an area of some 2000 km^2 combining helicopter-borne time-domain EM with a magnetic and gamma-spectrometry survey. Here we describe the survey planning, quality control (QC) and processing, and initial interpretation phases highlighting the findings and value we gained from the data.

Survey area

The AEM survey area is located in the Republic of Mozambique within the onshore Inhaminga block situated north of Beira and south of the Zambezi River. The Inhaminga block covers an area of 16 500 km^2 and is located some 200 km from Sasol's development of the Pande and Temane gas fields (Figure 1*a*). The AEM survey covers an area of roughly 50 × 40 km located in the northern area of the licence, close to Inhaminga. Main flight lines are ~45 km long heading NW–SE with 500-m line spacing.

Geology

The AEM survey covers a portion of the Urema Graben in the northern part of the Inhaminga licence (Figure 1*b*). The graben was formerly interpreted to represent the southernmost part of the East African Rift, but new seismic surveys show the main rift period of the Urema Graben to be Mesozoic in origin. Only a thin portion of the graben fill can be ascribed to the East African Rift episode (the sequence above the Oligocene in Figure 1*c*). The Urema Graben forms a half-graben with the main fault located just west of the Inhaminga High. Several transfer faults intersect the graben within the survey area, and evidence of transpression and inversion can be seen on the seismic data. The mid-graben high

 10.1071/EG09011 0812-3985/09/030001

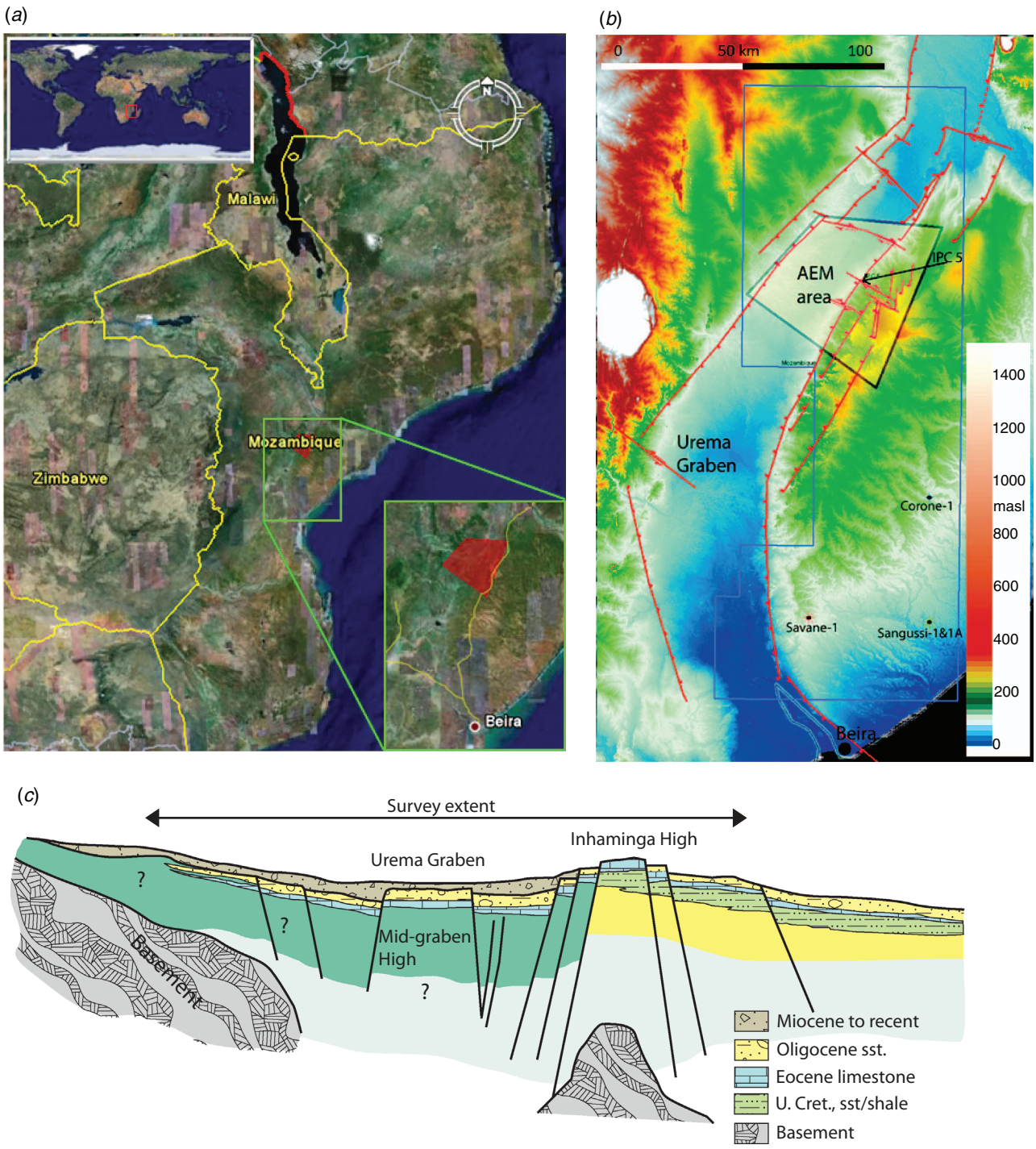

Fig. 1. (*a*) Geographic location of the survey area in red (map and image taken from Google Earth™ mapping service), (*b*) Regional topography indicating the AEM survey area and borehole IPC-5 with respect to the Urema Graben. Outline of the Inhaminga licence block in blue. (*c*) Cross section through the Urema Graben indicating the geological setting of the survey area.

(shown in Figure 1*c*) formed as a result of this late tectonic activity. Exploration drilling in the 1930s proved gas in the IPC-5 well up on the Inhaminga High, and there are several reports of possible seeps along the eastern graben margin. However, no seeps have been confirmed from the graben interior so far. The near surface geology is fairly well known from the Inhaminga High and eastward. The Eocene Cheringoma Formation (Fm) is exposed in the most elevated areas and in river cut valleys associated with the Inhaminga High. This formation comprises shallow marine limestones with interbeds of siliciclastic sandstones. Going east, the Cheringoma is overlain by the Oligocene-Miocene Limpopo Fm (Figure 2), consisting of immature coarse grained siliciclastics and mudstones. The near surface stratigraphy in the graben interior is more uncertain. Recent fluvial and alluvial sediments cover the relatively thin East African Rift fill. Still within the AEM penetration depth, we interpret the Inharime Fm and the Cheringoma Fm to be present below this young sequence, (Figure 1*c*). In the Lower Zambezi graben to the north of the study area, alkaline volcanics are present between the Mesozoic syn-rift sediments, and we cannot rule out the possibility of Cretaceous volcanics within the Urema Graben as well.

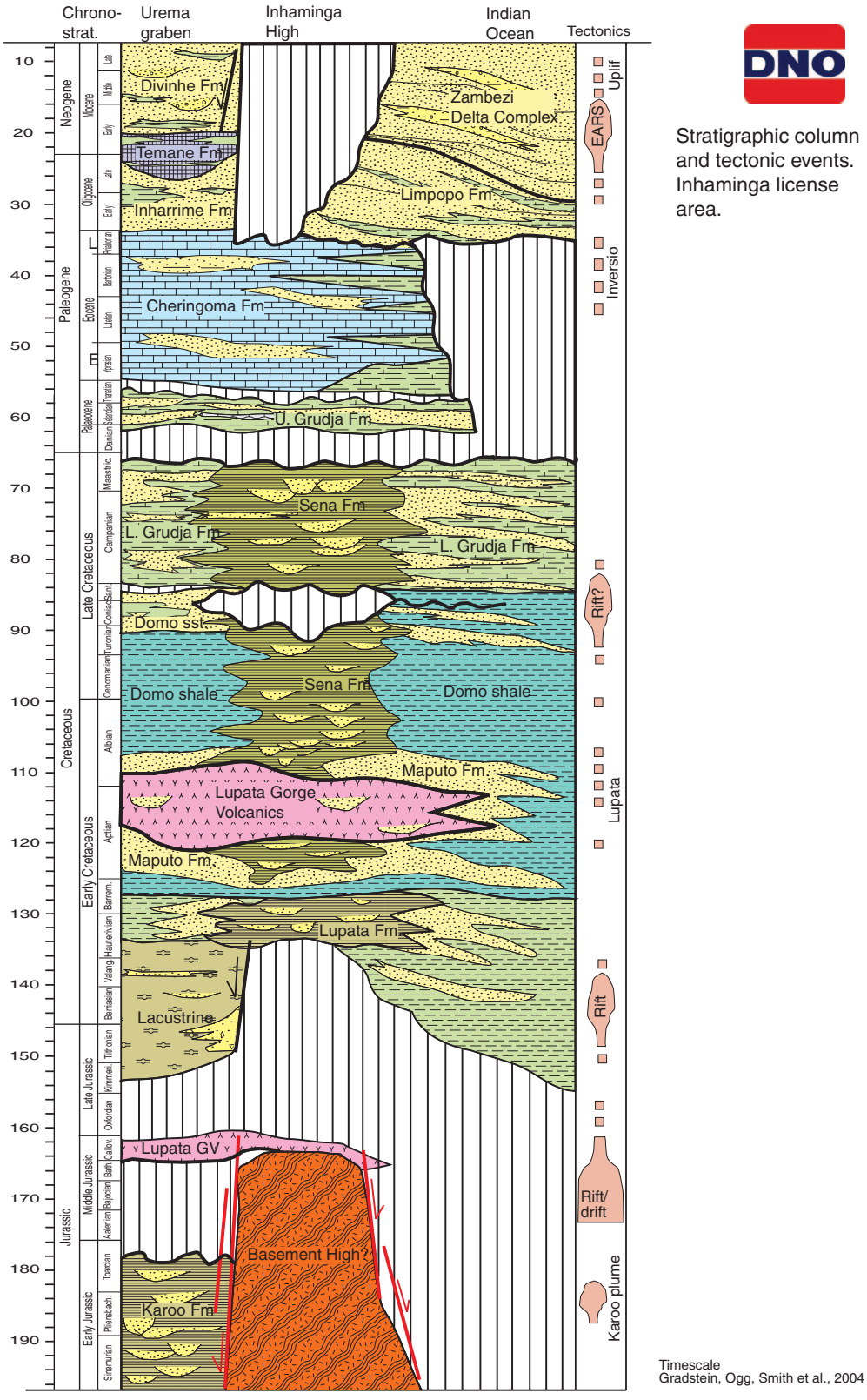

Stratigraphic column and tectonic events. Inhaminga license area.

Fig. 2. Stratigraphic column and tectonic events, Inhaminga licence area.

Exploration concept

Exploration drilling in recent years has been concentrated in the south-eastern corner of the licence, chasing a Pande-Temane type of play (the Corone-1, Savane-1 and Sangussi-1&1A wells, Figure 1*b*). This was partly due to the legacy from previous operators, and the fact that this was the only play covered with seismic data. Unfortunately, the drilling was unsuccessful with only minor gas shows. The exploration focus was consequently shifted to the Urema Graben and Inhaminga High on the eastern graben margin. In 2006, DNO International conducted two parallel geochemical surveys covering the graben margin close to Inhaminga city in addition to the graben area west of Inhaminga. Both surveys were designed as screening-surveys, covering a relatively large area with large spacing between each

sample, (spaced roughly 2 km along selected transects meandering through the area). However, the results of these surveys were encouraging, and triggered further work in the area. They both indicated gas anomalies along the Inhaminga High, and oil anomalies within the graben. In 2007 DNO acquired a limited 2D seismic survey west of Inhaminga city. This was the first seismic survey ever to cross the Urema Graben in Mozambique. The IPC-5 well (Figure 1*b*) from 1935 reportedly flowed gas, and gas is seeping to the surface at several places along the main bounding fault. This highlighted the Inhaminga High as a promising target for gas exploration. The existing seismic survey covers only parts of the Inhaminga High, but using the surface relief from the digital terrain model in combination with geological mapping on the ground, a total relief for the structure of minimum 200 m can be calculated for the Eocene Cheringoma Fm. It is likely that the possible reservoir units in the Upper Cretaceous have a similar relief. In 2008 it was decided to conduct an AEM survey over the most promising exploration targets on the licence. This includes the Inhaminga High, as well as the areas in the graben with 'oil signatures' from the two independent geochemical surveys. The main motivation for the survey was to confirm seepage of hydrocarbons to the near-surface sediments and rocks.

Geophysical target

Hydrocarbons which migrate from buried source rocks and reservoirs all the way to the surface (seepages) interact with the near surface geology, e.g. cause alteration effects in mineralogy and pore water in limestones and clastic rocks. Further, seepage-associated bacterial activity appears to have the potential of skewing the local geochemistry. These alterations potentially create anomalies in the physical properties of the rocks especially in resistivity and chargeability. Sternberg (1991) describes the mechanisms leading to resistivity anomalies in detail. It is noteworthy that alteration halos may show as a resistive or conductive feature. As described above, the geological setting sets the base for a successful AEM alteration zone mapping survey, e.g. the near surface comprises limestone and sandstone in an area of expected seepage.

It is further likely that magnetite, potassium or uranium concentrations may be changed through the alteration processes producing anomalous magnetic and/or gamma ray spectrometer responses. Saunders et al. (1994) reported correlations between Potassium/Thorium and Uranium/Thorium ratios and oil and gas fields in Australia and Texas (Saunders et al., 1993). Magnetic anomalies have been linked to petroleum deposits by some authors but also the opposite has been reported. Machel and Burton (1991) studied the chemical and microbiological processes capable of causing anomalous magnetisations related to hydrocarbon accumulations. Liu et al. (2006) analysed some 50 well samples and found significant enhancements in susceptibility and magnetisation. Busby et al. (1991), however, analysed magnetic data and borehole cuttings from an oilfield in the UK and concluded, that the sporadically observed magnetic anomalies were caused by well casings, rather than mineral alteration effects.

Airborne geophysical methods

The very limited prior knowledge about the expected resistivities, and furthermore whether a conductive or resistive target was to be mapped, made us choose a universal helicopter-borne time domain system. A time domain system was selected for its superior bandwidth and resolution in comparison to frequency domain systems. Densely sampled and accurate off-time channels give rise to EM inversion models with higher vertical resolution than limited frequency domain data. Further we did not expect to meet highly resistive ground and very near surface features, which would only be resolved by frequency domain systems (Steuer et al., 2009). Penetration depth was not the ruling factor but rather lateral and depth resolution, which led to a helicopter-borne system. In comparison to helicopter towed EM platforms, fixed wing EM systems achieve higher penetration depths by virtue of high transmitter moments, but at the same time have larger footprints due to their higher nominal altitude and induction geometry (Reid and Vrbancich, 2004).

Helicopter time domain EM

Given the limited knowledge about target properties or geometry we saw the need for a helicopter-borne instrument with multiple channels and receiver orientations. As the seepage targets might be vertically oriented along fault planes, a horizontal receiver seemed necessary. Providing a total of 50 time channels including on- and off-time (spanning from 77 μs to 4.5 ms after turn off) for both vertical and horizontal receiver coils, our choice was the AeroTEM IV platform provided by Aeroquest Ltd, Mississauga, Canada. Further specifications on the HEM system are provided in Table 1 and Figure 3.

Fixed wing magnetic gradiometer and spectrometer

For logistic reasons, and to achieve higher resolution than with a helicopter-based package, the radiometric survey was carried out from a fixed-wing platform provided by Aeroquest's sister company UTS Geophysics, Perth, Australia. Both platforms carried magnetometers, yet the fixed wing system was flying a horizontal gradiometer array. The gradiometer consisted of three Scintrex CS-2 cesium vapour magnetometers (0.01 nT sensitivity, 10 Hz sample rate) attached to the wing tips and a tail stinger on a PAC750-XL and a three component fluxgate vector magnetometer. The aircraft was further carrying an Exploranium GR-820 spectrometer featuring two 16.8 L detector packs delivering 256 channels at 1 Hz.

Results

As first results had to be provided on a tight schedule, extensive daily QC and processing was crucial during the roughly 5-week survey period (July/August 2008). Additionally to production data, QC data included drift and calibration ascends to judge the system-response noise envelope. Transmitter performance was continuously monitored and supplied with the EM data. Knowledge of the stability of the transmitter is crucial for high

Table 1. Technical specifications of the used helicopter time-domain EM system (AeroTEM IV).

Transmitter waveform	Triangular pulse shape, base frequency 75 Hz
Transmitter on-/off-time	2.06 ms on/6 ms off
Trasnmitter loop	12 m diameter, five turns
Peak current/dipole moment	420 A/240 kNIA
Receivers	2 receiver coils vertical (Z) and horizontal (X)
Receiver position	Horizontal offset from Tx loop centre 1 m and 4.8 m for X and Z respectively
Data acquisition	Digital recording on board the helicopter with 36 kHz. Streaming data stacked to 10 Hz EM data
Towing geometry	Towing cable length 50 m, nominal EM bird height 40 m above ground, Magnetometer bird 29 m above EM bird

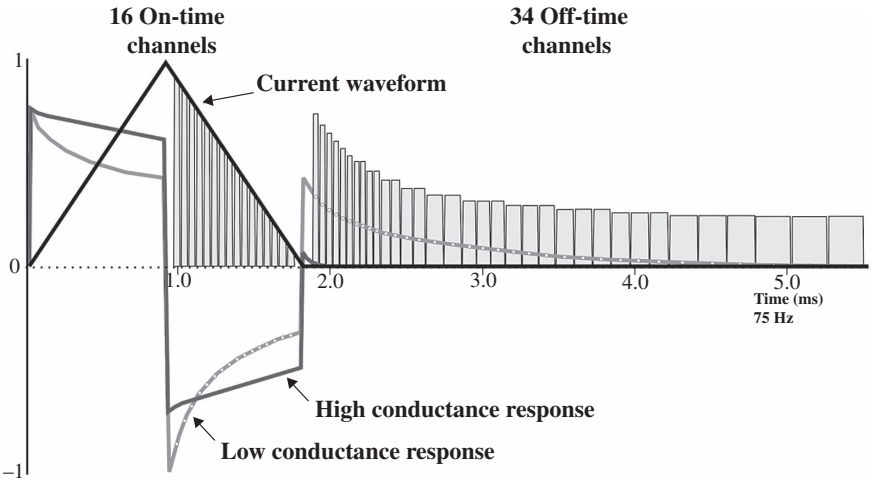

Fig. 3. Helicopter time domain EM transmitter and receiver waveforms (AeroTEM IV), black line depicts transmitter wave form, grey lines illustrate schematic receiver responses. On-time data is acquired during ramp-up and -down and stacked to one segment.

quality inversion results. The system used for this survey showed no particular problems, shape and moment of the transmitter pulse remained stable. However, the absolute timing of the transmitter pulse with respect to the processed time gates changed by up to 20 µs from flight to flight (Table 2). During each flight the timing was generally very stable with standard deviations of some 0.05 µs (Table 2). Further, a roughly 2-km-long test line was surveyed daily to control data repeatability. Even though moderate delivery delays occurred due to the remoteness of the field camp, daily data provided the timely chance to flag survey lines for re-flight and to extend the survey area during acquisition. A promising anomaly pattern was identified during acquisition, which led to the extension of the survey area for some 15 km to the South.

Magnetics

Prior to levelling, the magnetic data was subjected to a lag correction and a spike removal filter. The filtered aeromagnetic data were then corrected for diurnal variations using the magnetic base station and the intersections of the tie lines. No corrections for the regional reference field (IGRF) were applied to the final magnetic data. The magnetic data were then levelled and reduced to the magnetic pole (RTP). RTP data were further processed to produce the first vertical derivative (1VD), which enhances magnetic features that occur in the relative near-surface at the expense of deeper sources. The second vertical derivative (2VD) was also calculated to enhance sources in the very near-surface (Figure 4).

We begin the interpretation of the magnetic data sources in the near-surface. The response amplitudes are quite low as might be expected from a sedimentary sequence. The response character, however, is quite distinct. The principal near-surface feature is a north-east trending linear to sinuous feature which transects the entire survey block (Line A–A in Figure 4). This feature suggests the presence of minor magnetic mineralisation associated with a north-east trending fault. This interpretation is supported by the digital terrain and radiometric datasets which both reflect this structure at surface. Other responses in the second vertical derivative image of note are a north-east trending fabric in the far north-east corner of the survey area. This fabric reflects minor magnetic mineralisation in the geological units. The north-east trend of the geology in this area is confirmed in the radiometric datasets. Other zones of magnetic activity in the 2VD image occur south-east of the fault structure mentioned above. These magnetically active areas correlate with a high uranium, low potassium, and moderate thorium unit mapped by the radiometric survey. The units appear to be erosionally resistant as they occur at the top of small topographic scarps. Two small circular sources along the south-west margin of the survey block occur in the near-surface. These sources may be small intrusive plugs or lamproites. This type of intrusive usually exploits structurally weak zones, so may be important indicators of the presence of faults or structural weakness in the area. The deeper sources are interpreted from the total field RTP and 1VD images. There are four dominant basement highs, one in each of the four corners (north, east, west, and south) of the survey. The eastern and southern sources appear to be connected with a relatively narrow high which extends with a north-east trend along the previously identified NE trending structure. This deeper source is offset to the NW of the near-surface expression of this fault, suggesting that the fault has a north-west dip, consistent with the geological section given above. These two highs suggest the presence of magnetic basement rocks beneath the Inhaminga High.

A magnetic low extends with a NE trend along the axis of the centre of the graben, but a second large magnetic low trend extends NW–SE through the centre of the survey area. This

Table 2. Snapshot of quality control data for the presented survey.

Tx_on, time stamp at transmitter ramp up; pulse, pulse width (transmitter on-time); peak, transmitter peak current; s.d., standard deviation of parameter.

Flight-number	Line-km	Tx_on [µs]	s.d. [µs]	Pulse [ms]	s.d. [µs]	Peak [kNIA]	s.d. [kNIA]
15	98	–10.9	0.08	2.065	0.8	239.4	0.1
16	104	–6.0	0.04	2.064	0.5	239.3	0.1
17	95	–10.7	0.05	2.062	0.2	239.1	0.1

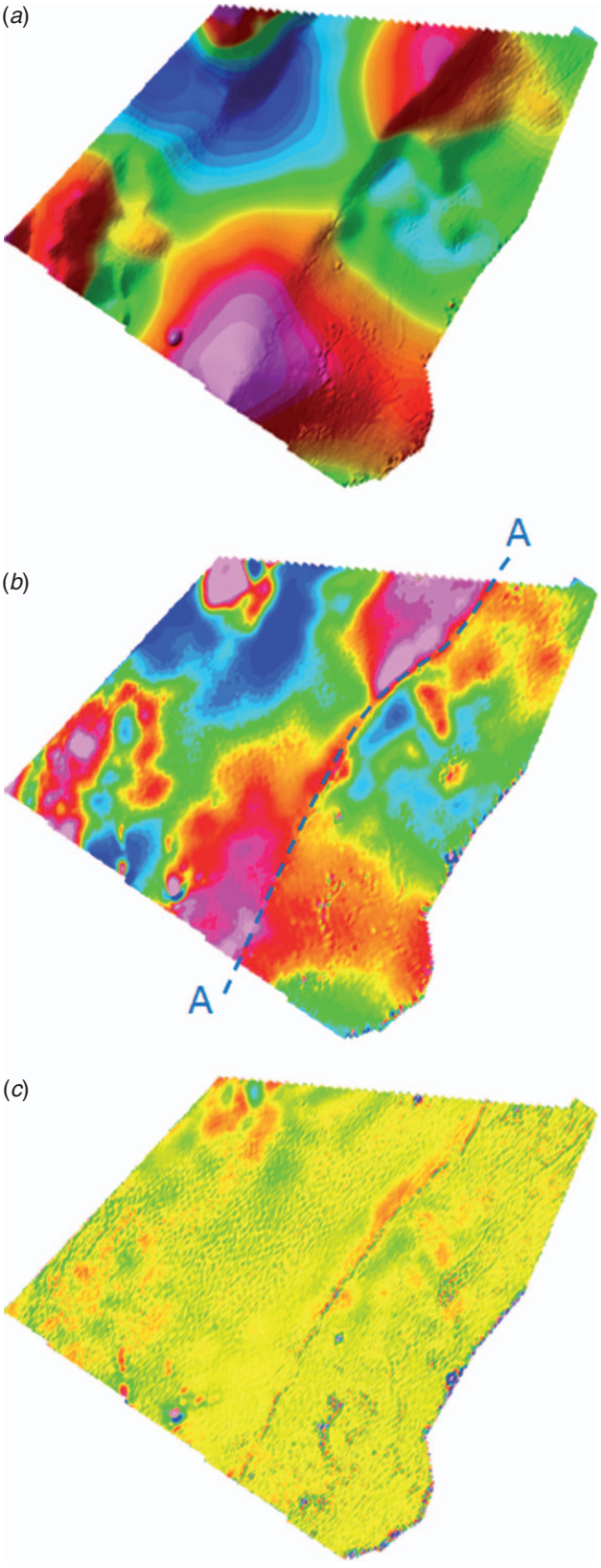

Fig. 4. (*a*) Magnetic data reduced to the magnetic pole (RTP) with shading from an azimuth of 315 degrees. (*b*) First vertical derivative of RTP, (*c*) Second vertical derivative of RTP. Line A–A: Graben bounding fault interpreted from magnetic data and topography.

low may indicate a major NW-trending structural zone, which is evident from NE-striking seismic lines in the area. A complex magnetic pattern in the magnetic response in the low SE of the major NE-trending structure supports the presence of a high level of structural activity.

Spectrometry

Radiometric data were corrected for dead-time, cosmic and aircraft background, radon background and height above ground according to International Atomic Energy Agency standards. Consequently stripping ratios were applied to the 256 channel data to determine corrected spectral windows for Thorium, Potassium and Uranium expressed in counts per second (Figure 5) and apparent radioelement concentrations. Uranium and total count were further tie-levelled to remove effects of residual radon background. Based on the apparent element concentrations we followed a normalisation approach suggested by Saunders et al. (1993). According to the authors a combination of relative Thorium-normalised Uranium and Potassium anomalies appeared to be associated with hydrocarbon seepage alterations of the very near surface. Described briefly, Saunders' method accounts for lithologic and related effects by the Thorium normalisation and then combines the expected decrease in relative Potassium and increase in relative Uranium to one value, dubbed DRAD. DRAD is determined by DRAD = (k Th)/K – (u Th)/U where U, K and Th are the measured concentrations of Uranium, Potassium and Thorium, respectively. The constants u and k scale the relative concentrations to the mean concentrations over the survey area (u = mean(U)/mean(Th), k = mean(K)/mean(Th)). We further define an inverse DRAD as [U/(u Th) – K/(k Th)].

In comparison to the ROIs in Figure 5, only two main areas appear anomalous in the resulting DRAP map (Figure 6*a*) in contrast to the reversed normalised inverse DRAP (Figure 6*b*) highlighting geological effects such as sedimentary units and the clearly visible NW-striking riverbeds. Note the consistency between the major magnetic lineament (line A–A in Figure 4) and the change from purple to reddish/greenish tones in the radiometric map, presumably associated with the bounding fault along the eastern graben margin.

EM resistivity

Raw streaming data was processed by the contractor to a final stage of compensated, filtered, stacked and levelled 50 time channels of horizontal and vertical EM data. The system features active bucking coils and primary field compensation is assessed by use of the routinely performed high altitude background checks. Final processed data were more consistent than the preliminary field data, especially for early- and late-time data. Note that EM data presented in Figure 7 depicts final data, whereas the inversion example in Figure 8 is based on preliminary data, as final data was not available at the time of inversion. Given the tight schedule of this project, further processing and interpretation needed to be started immediately following survey completion. Some initial inversion runs with a standard Marquardt-style layered earth inversion algorithm have been performed using EMIGMA V8.1 (Murray et al., 1999). The presented model section in Figure 8 is based on a five layer inversion with logarithmically increasing starting model layer thickness and a homogeneous resistivity of 30 Ωm. No lateral constraints were applied. Off-time data channels 4 to 28 have been used for inversion (144 μs to 2.9 ms) to avoid noisy early- and late-times in the preliminary data.

Two main structures show up on the raw EM data: A strong SW–NE-striking anomaly in the central part of the graben and smaller anomaly band along the eastern graben margin. Let us first discuss the central anomaly. Its eastern edge appears at the same position from early to late time-channels. This suggests an abrupt

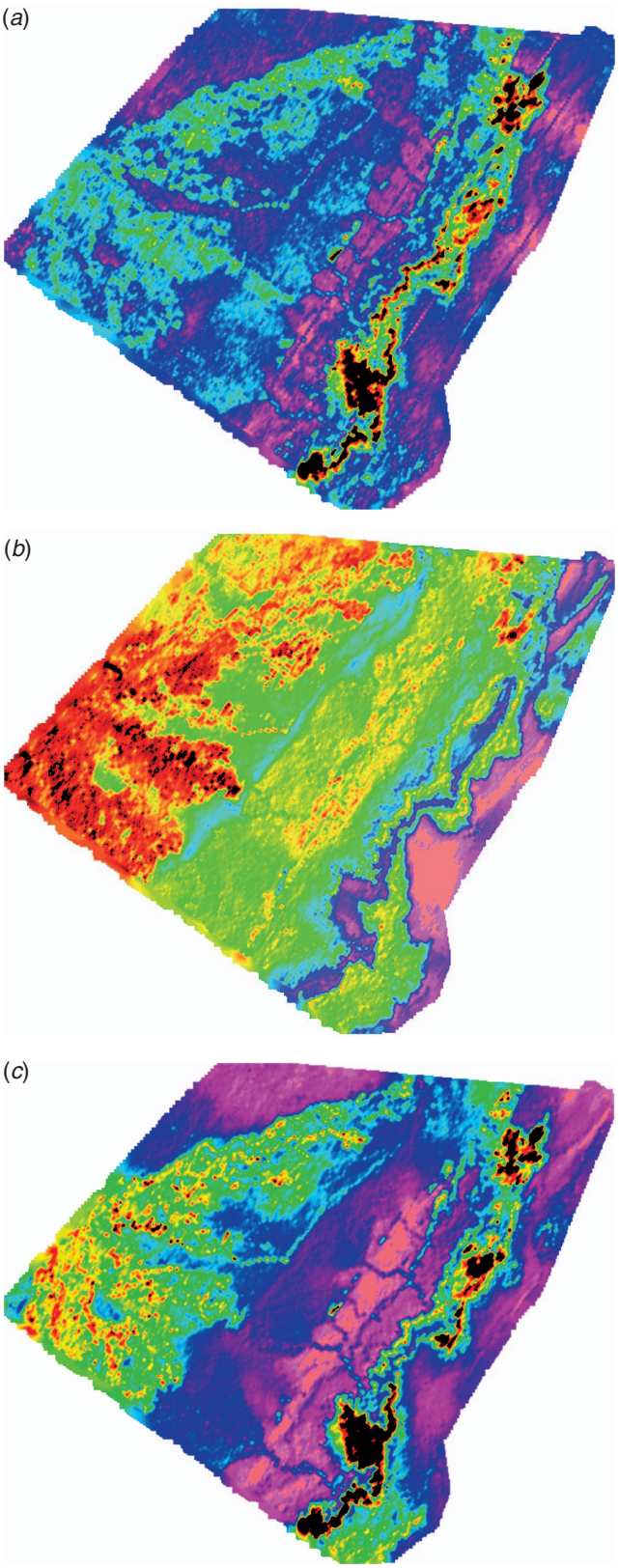

Fig. 5. Spectrometry maps: (*a*) Uranium, (*b*) Potassium, (*c*) Thorium concentration all in counts per second, colour-scales from purple for low to red for high counts.

lateral termination of the conductive unit and probably reflects a fault along this eastern edge. Seismic lines crossing the anomaly indicate a different sedimentary regime outlined by the EM anomaly likely an overprint of the Mid-graben High in Figure 1*c*. The post-Eocene transpression has lifted older rocks nearer to the surface in the middle of the graben, west of the Inhaminga High. This might explain the strong anomaly seen in this position (Figure 7*a*). The western anomaly edge's position migrates towards the east in the later time-channels, suggesting an easterly dip and/or a thickening of the conductive unit towards the east. The apparent resistivity product (Figure 7*b*) outlines a rather homogenous near-surface in the western survey area. This may indicate a resistive unit at depth, dipping SE and overlain by conductive sediments (maybe Miocene East African Rift graben fill, Figure 1*c*) identified in the apparent resistivity map. Consequently the conductive unit thickens towards the East, leading to an increased cumulative conductance and thus giving rise to an increased response in the EM data. In the East the stratum is spontaneously cut off by the central graben high. In the central eastern part of the survey area (~N7 960 000 E7 10 000), the Inhaminga High, known to consist of massive Cheringoma limestone, features as a high apparent resistivity zone, as one would expect. Another resistive feature in Figure 7*b* as well as the anomaly band along the eastern graben margin will be mentioned in the next section.

Discussion

While the general regional and structural interpretation of especially the magnetic data was addressed above, we want now to focus on the goal of the survey – outlining potential hydrocarbon seepage zones form the airborne data.

During field work in 2008 an active gas seep was observed and sampled in the very south of the survey area. The general geological concept is that the main fault zone of the half-graben, leads the way for hydrocarbon seepage from the host or reservoir rock at great depth all the way to the surface. The main faults are evident from the eastern graben margin topography, where the Inhaminga High drops to the Urema Graben via two or more escarpments of up to 100 m. Consequently the EM fingerprint at that area is of highest interest. In fact, the sinuous anomaly that features in EM and radiometric data along the escarpment of the Inhamninga plateau appears to have a causal connection to the observed seepage area. Let us compare the signature of that area in the three maps provided in Figures 6*a* and 7. The EM response is relatively high just on the foot of the escarpment (green in Figure 7*a*). Apparent resistivity is consequently low in that area (red in Figure 7*b*). West of the first drop an anomalously high apparent resistivity is indicated until the next escarpment (blue in Figure 7*b*). The normalised radiometric data indicates potentially seepage related alterations in the same area (red in Figure 6*a*). Also the magnetic data (second vertical derivative in Figure 4) indicates a magnetically active area. One exemplary inverted depth section (Figure 8) provides further insight. The approximate location of the inverted section is marked with a yellow-red line on the EM data map (Figure 7*a*). The resistive anomaly (Figure 7*b*) has a rather shallow source (a roughly 50-m thick layer some metres below the surface), the conductive response (Figure 8) seems to be caused by a near surface shallow layer at the foot of the escarpments. A subset of 10 lines in this area has been inverted at this stage, showing a consistent extent of both surface conductive and shallow resistive structure. The selected inversion example is coincident with a seismic line, extending further into the graben and to the East (red line in Figure 7*a*). In the seismic section an area of dimmed reflections is evident and coincides with the conductive anomaly. A possible explanation for dimming of seismic reflections could be gas seepage along the faults in this area. The coincidence of seismic dimming, AEM and radiometric anomaly makes us confident of having identified a seepage alteration zone.

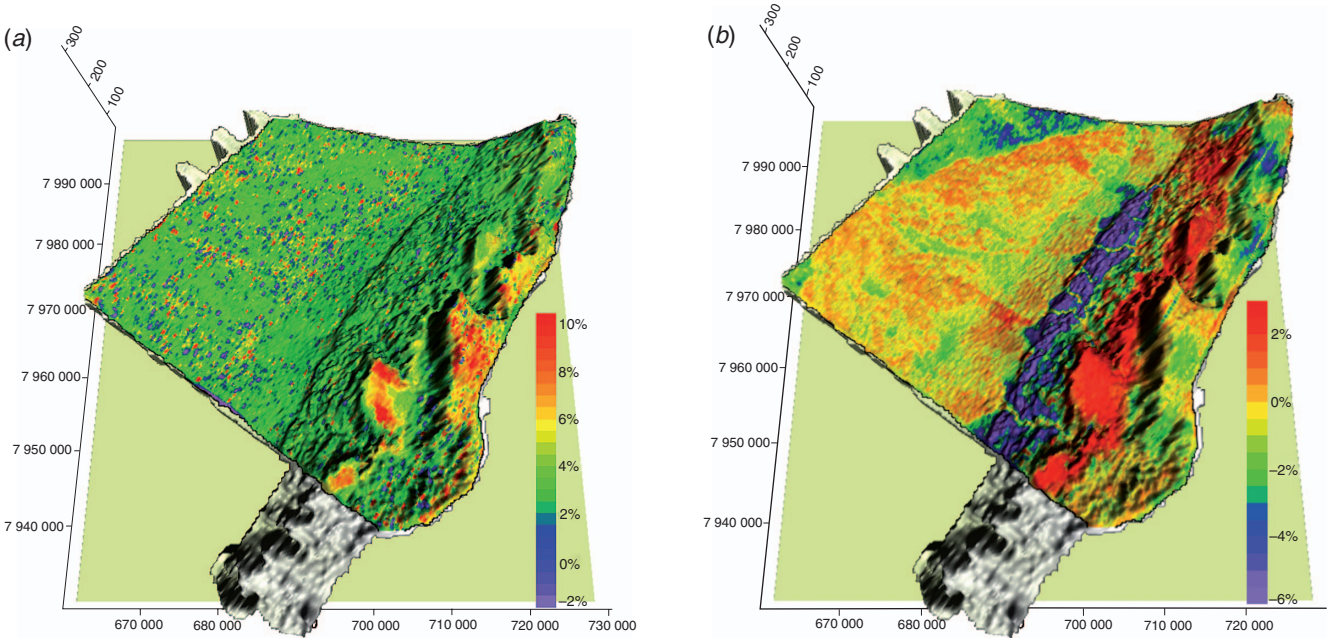

Fig. 6. (*a*) Radiometric data presented as combined relative Uranium and Potassium anomaly normalised to Thorium (*DRAP* after Saunders et al., 1993) highlighting potential alteration plumes draped over topography with shading from an azimuth of 139 degrees. (*b*) Inverse *DRAP* highlighting near surface geology expressions. Geographic coordinates are given in UTM 32S Easting (x) and Northing (y).

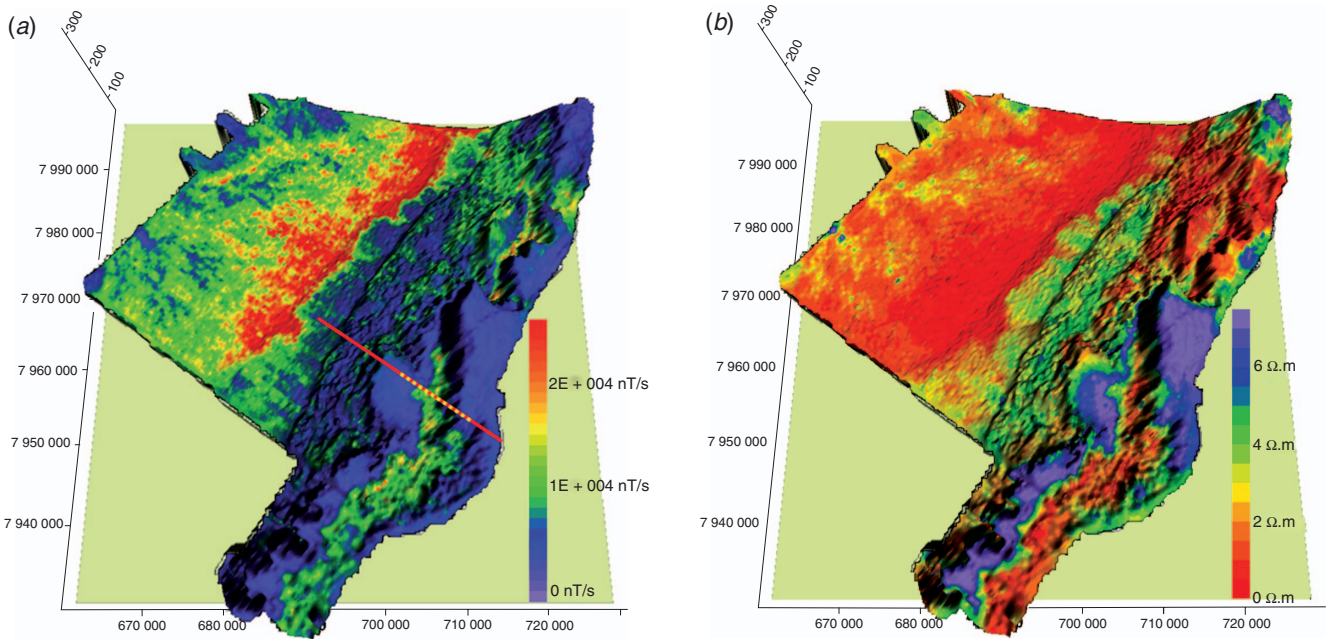

Fig. 7. (*a*) Airborne EM response, raw data: Off-time channel #4 (0.160 µs after turn-off) vertical component draped over topography. The red line indicates position of seismic profile and inversion section (yellow-red dashed). (*b*) Airborne EM response, secondary data: Early time apparent resistivity derived via pseudo-layer half-space model (Huang and Rudd, 2008) draped over topography. Geographic coordinates are given in UTM 32S Easting (x) and Northing (y).

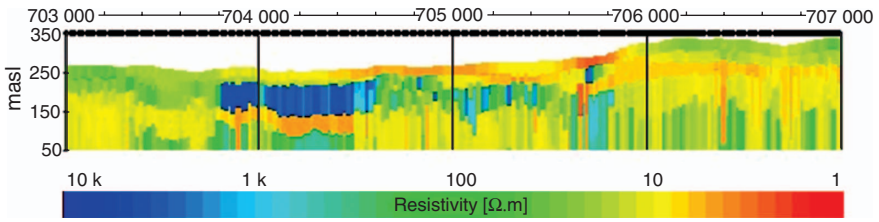

Fig. 8. Resistivity depth section along 4.9 line km indicated in Figure 7*a* with yellow-red line. Determined with Marquard-style 5-layer inversion without lateral constraints. *x*-axis coordinates are UTM 36S Easting along survey line.

Conclusion

Even though we have found abundant evidence for anomalous geophysical footprints, possibly caused by alteration halos, detailed follow up is needed to understand the complete geological situation. As an example, observed resistivity anomalies could be caused by alteration or just as well by common geology (e.g. clay layer overlaying limestone). However, this multi-method airborne geophysical survey proved highly valuable to outline general geological features and extrapolate information based on the limited seismic data.

Further geological interpretation of the geophysical data is ongoing. A 2D seismic survey is scheduled for the 2009 field season to gain more detailed structural understanding of the region. The exploration licence for the Inhaminga block has recently been renewed and the AEM survey has significantly contributed to the decision making process regarding the value of the area. Further exploration activities such as seepage sampling field work are planned based on the outcome of the airborne survey.

Acknowledgements

We are most grateful to DNO International ASA for initiating and funding this study and for giving permission to publish these results from an active exploration licence. Excellent communication and cooperation with the contractors Aeroquest Ltd and UTS Geophysics was highly appreciated. AAP is highly grateful to Ross W. Groom of PetrosEikon Inc., Canada for extensive scientific advice during all stages of this project.

References

Busby, J. P., Peart, R. J., Green, C. A., Ogilvy, R. D., and Williamson, J. P., 1991, A search for direct hydrocarbon indicators in the Formby area: *Geophysical Prospecting*, **39**, 691–710. doi: 10.1111/j.1365-2478.1991.tb00336.x

Huang, H., and Rudd, J., 2008, Conductivity-depth imaging of helicopter-borne TEM data based on a pseudolayer half-space model: *Geophysics*, **73**, F115–F120. doi: 10.1190/1.2904984

Hughes, L., 1983, Case Histories of an Electromagnetic Method for Petroleum Exploration: Proprietary data sale, Zonge Engineering & Research Organization. Available online at: www. www.zonge.com/ApplicationPetroleum.html [accessed 1 July 2009]

Liu, Q. S., Chan, L. S., Yang, T., Xia, X. H., and Cheng, T. J., 2006, Magnetic enhancement caused by hydrocarbon migration in the Mawangmiao Oil Field, Jianghan Basin, China: *Journal of Petroleum Science Engineering*, **53**, 25–33. doi: 10.1016/j.petrol.2006.01.010

Machel, H. G., and Burton, E. A., 1991, Chemical and microbial processes causing anomalous magnetization in environments affected by hydrocarbon seepage: *Geophysics*, **56**, 598–605. doi: 10.1190/1.1443076

Murray, I. R., Alveraz, C., and Groom, R. W. 1999, Modelling of Complex Electromagnetic Targets Using Advanced Non-linear Approximator Techniques: *Expanded Abstract*, SEG Annual Meeting.

Reid, J. E., and Vrbancich, J., 2004, A comparison of the inductive limit footprints of airborne electromagnetic configurations: *Geophysics*, **69**, 1229. doi: 10.1190/1.1801939

Saunders, D. F., Burson, K. R., Branch, J. F., and Thompson, C. K., 1993, Relation of thorium-normalized surface and aerial radiometric data to subsurface petroleum accumulations: *Geophysics*, **58**, 1417–1427. doi: 10.1190/1.1443357

Saunders, D. F., Branch, J. F., and Thompson, C. K., 1994, Tests of Australian aerial radiometric data for use in petroleum reconnaissance: *Geophysics*, **59**, 411–419. doi: 10.1190/1.1443603

Smith, R. S., and Rowe, J. D., 1997, A new regional exploration method for detecting hydrocarbon alteration plumes: the ALTREX™ method: *Exploration Geophysics*, **28**, 286–291. doi: 10.1071/EG997286

Sternberg, B., 1991, A review of some experience with the induced-polarization/resistivity method for hydrocarbon surveys: Successes and limitations: *Geophysics*, **56**, 1522–1532. doi: 10.1190/1.1442963

Steuer, A., Siemon, B., and Auken, E., 2009, A comparison of helicopter-borne electromagnetics in frequency- and time-domain at the Cuxhaven valley in Northern Germany: *Journal of Applied Geophysics*, **67**, 194–205. doi: 10.1016/j.jappgeo.2007.07.001

Manuscript received on 17 February 2009; review received June 15, revision submitted June 30.